arXiv:1410.3190v3 [cond-mat.mes-hall] 28 Jul 2015

Stochastic model showing a transition to self-controlled particle-deposition state induced by optical near-fields

Kan Takahashi [*], Makoto Katori [†], Makoto Naruse [‡], Motoichi Ohtsu [§]

28 July 2015

Abstract

We study a stochastic model for the self-controlled particle-deposition process induced by optical near-fields. This process was experimentally realized by Yukutake et al. on an electrode of a novel photovoltaic device as Ag deposition under light illumination, in which the wavelength of incident light is longer than the long-wavelength cutoff of the materials composing the device. Naruse et al. introduced a stochastic cellular automaton model to simulate underlying nonequilibrium processes which are necessary to formulate unique granular Ag film in this deposition process. In the present paper, we generalize their model and clarify the essential role of optical near-fields generated on the electrode surface. We introduce a parameter b indicating the incident light power per site and a function representing the resonance effect of optical near-fields depending on the Ag-cluster size on the surface. Numerical simulation shows a transition from a trivial particle-deposition state to a nontrivial self-controlled particle-deposition state at a critical value $b_{\rm c}$, and only in the latter state optical near-fields are effectively generated. The properties of transition in this mesoscopic surface model in nonequilibrium are studied by the analogy of equilibrium phase transitions associated with critical phenomena and the criteria of transition are reported.

1 Introduction

Nanophotonics, which investigates light-matter interactions on the nanometer scale, has been intensively studied from a variety of aspects ranging from fundamental interests, such

[*]Department of Physics, Faculty of Science and Engineering, Chuo University, 1-13-27 Kasuga, Bunkyo-ku, Tokyo 112-8551, Japan; e-mail:k-takahashi@phys.chuo-u.ac.jp

[†]Department of Physics, Faculty of Science and Engineering, Chuo University, 1-13-27 Kasuga, Bunkyo-ku, Tokyo 112-8551, Japan; e-mail:katori@phys.chuo-u.ac.jp

[‡]National Institute of Information and Communications Technology, 4-2-1 Nukui-kita, Koganei, Tokyo 184-8795, Japan

[§]Nanophotonics Research Center, Graduate School of Engineering, The University of Tokyo, 2-11-16 Yayoi, Bunkyo-ku, Tokyo 113-8656, Japan

as atom and optical near-field interactions [1, 2, 3], to applications including environment and energy [4, 5], healthcare [6], solid-state lighting [7], information and communications technologies [8, 9], among others. Precision control of the geometrical features, such as the size, layout, morphology, at the nanometer scale are important in realizing valuable functionalities [1, 3]. In this context, the nanophotonics fabrication-principles and techniques have been providing interesting and important light-assisted, self-controlled nanostructures; nanoparticle array formation [10], light emission from indirect-transition-type semiconductors (such as silicon) [7], appearances of photosensitivity at wavelengths longer than the long-wavelength cutoff [5], etc. In these light-assisted material formations, while elemental physical processes indeed involve optical near-field interactions at the nanometer-scale, the system is open to environment and thus is accompanied with energy flow and environmental fluctuations. For these systems, stochastic modeling [11, 12] is very useful in order to obtain deeper understandings of the underlying physical processes as well as to gain design principles for future devices and systems [3]. In the present paper, we develop the cellular automaton model [13] proposed by Naruse et al. [14], which was introduced to simulate self-controlled pattern formation of Ag film reported by Yukutake et al. [5] on the electrode of their photovoltaic device.

Figure 1 shows the cross-sectional structure of the photovoltaic device of poly-(3-hexyl thiophene) (P3HT) and ZnO sandwiched by Ag and indium tin oxide (ITO) electrodes. A P3HT layer (about 50 nm thick) and a ZnO layer (about 100 nm thick) are used as p-type and n-type semiconductors, respectively, and an ITO film (about 200 nm thick) and an Ag film (a few nanometers thick) are used as two electrodes. This multi-layered film with an area of 30 mm^2 is deposited on a sapphire substrate in series. At the last stage of the fabrication process of the multi-layered device, Ag was deposited on the Ag thin film. The Ag is deposited by radio frequency (RF) sputtering under light illumination while applying a reverse bias DC voltage, $V_b = -1.5$ V, to the P3HT/ZnO p-n junction. The wavelength of the incident light is 670 nm, which is longer than the cut-off wavelength $\lambda_c = 570$ nm of P3HT. Under light illumination, optical near-fields are locally generated on the Ag surface. They induce coherent phonons and form a coupled state with them, which is called a *virtual exciton-phonon-polariton* [15] or the *dressed-photon-phonon (DPP)* [3]. If the DPP field extends to the p-n junction, the two-step excitation process of electrons occurs (see [5] and Sec.7.2.1 of [3]) and then electron-hole pairs are created at the p-n junction. As illustrated by Fig. 2, by the reverse bias voltage, the electrons and holes are separated from each other. The positive holes are attracted to the Ag film, which make the Ag film be positively charged. It was argued in [5, 14] that due to randomness in Ag deposition process by RF sputtering, the density of Ag deposits will spatially fluctuate. Since the optical near-fields are generated by short-ranged light-matter interaction, the optical near-fields will also become spatially inhomogeneous in the film. In the local area of the Ag surface, where the optical near-field is effectively induced, more positive holes are generated and transferred into the area. In such an area, which is more positively charged than other areas, the subsequent deposition of Ag will be suppressed, since the sputtering Ag is positively ionized by passing through the argon plasma used for RF sputtering. Such a feedback mechanism induced by optical near-fields will lead to the unique and nontrivial granular structure of the Ag film and such

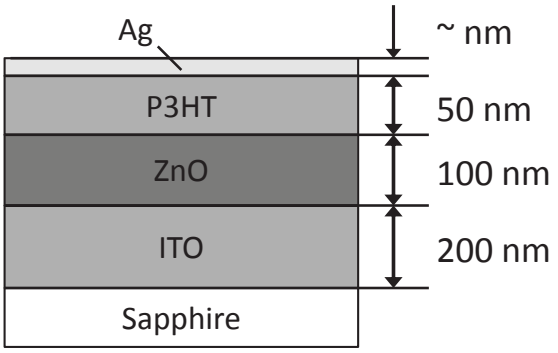

Figure 1: Cross-sectional structure of the photovoltaic device of Yukutake et al.[5].

a self-controlled pattern formation was indeed observed in experiments [5].

Naruse et al. [14] introduced a stochastic cellular automaton model on a square lattice [13] such that each cell has one of the two values 0 and 1, which represents a vacancy and an occupation by an Ag grain, respectively. Time evolution of Ag clusters in random deposition of Ag^+ grains on a lattice has been numerically simulated. It was assumed in their model that the repulsive force acting on an Ag^+ grain when it is deposited on a site in the lattice is simply proportional to the total number of occupied sites in the eight neighbors (*i.e.* the Moore neighborhood in the square lattice). This model works well as a minimal model for the inhomogeneous pattern formation of Ag film on an electrode of the photovoltaic device, while a role of spatially inhomogeneous charge-distribution due to the heterogeneous effect of optical near-fields was not clarified.

In the present paper, we propose a nonequilibrium statistical-mechanics model on an $L \times L$ square lattice Λ_L, in which two kinds of stochastic variables at each site $\mathbf{r}$ evolve in discrete time $t \in \{0, 1, 2, \dots\}$; the number of deposited grain on the site $n_t(\mathbf{r})$ and the amount of charge per site $q_t(\mathbf{r})$. These two variables are dynamically coupled as explained below. It is known that the effective potential of optical near-field is well-described by a Yukawa function of a distance r, $V_{\rm eff}(r) = e^{-r/\alpha}/r$. Here the interaction range α is proportional to the size of the matter which generates the optical near-field under light illumination [3]. In the present situation, the range α will be approximately equal to the size s of Ag-clusters. Hence growth of sufficiently large clusters is required in order to realize the situation such that the optical near-fields generated on the Ag surface reach the p-n junction and electron-hole pairs are created (see Fig.2). As a result, the charge increment of a cluster of Ag-deposited sites depends on the cluster size s, which is a functional of $\{n_t(\mathbf{r})\}_{\mathbf{r}\in\Lambda_L}$. We introduce a characteristic size s_0 of the cluster at which the charge increment of a cluster caused by the optical near-fields is maximized. Moreover, we assume existence of a characteristic size-

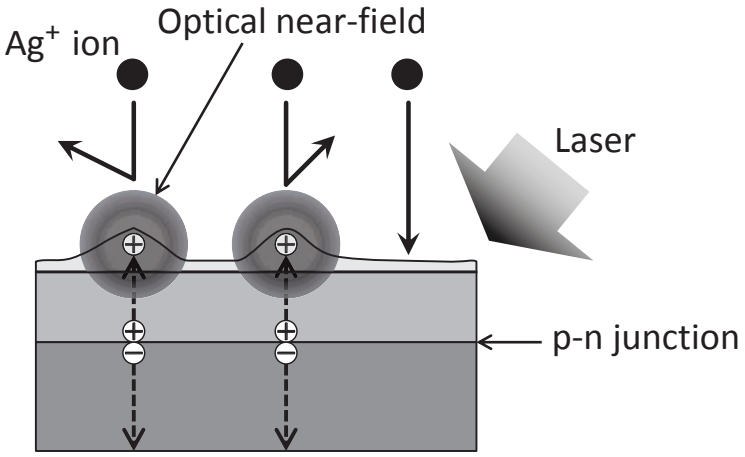

Figure 2: Under light illumination, an optical near-field is locally generated on the Ag surface, which induces a coherent phonon at the p-n junction. Then, this generates an electron-hole pair at the p-n junction, and by the reverse bias voltage, the positive hole is attracted to the Ag film on the surface, which makes the Ag film positively charged more. Subsequent deposition of Ag^+ ion on the electrode is suppressed by positive charge accumulated in the Ag clusters on the surface.

variation σ^2 such that if the cluster size s deviates from s_0 by much larger than σ, that is, if $(s - s_0)^2 \gg \sigma^2$, then the effect of the optical near-fields for charging cluster becomes very small. These assumptions are due to the basic property of DPPs, the optical near-fields coupled with phonons, called the *size-dependent resonance*, and here we use the Gaussian function

$$f(s) = \exp\left[-\frac{(x - s_0)^2}{2\sigma^2}\right] \tag{1.1}$$

to represent such size dependence (see Fig.2.6 in Sec.2.2.2 of [3]). Furthermore, in our numerical simulation, we perform exact calculation of long-ranged repulsive Coulomb interaction between the Ag^+ grain being deposited on a site and positively charged Ag clusters formed on the surface.

The main result of our numerical simulation of the model is that, when the lattice size L is large but finite, there are following two distinct mesoscopic states.

State A : If Ag clusters on the surface are formed with a proper size s such that $(s-s_0)^2 \leq \sigma^2$, then the optical near-fields are induced effectively to increase the charge of clusters and hence the total positive charge on the surface increases monotonically in time. It causes strong suppression of further deposition of Ag^+ grains on the surface and then the deposition will be stopped. As a result, a nontrivial and unique Ag film is formed.

State B : If sizes of Ag clusters on the surface tend to deviate from s_0 by more than σ, the optical near-fields are not induced effectively. In this case the charge on surface

will be saturated at a low level, and the suppression of deposition of Ag^+ grains on the surface remains weak. Hence the random deposition process will continue without any self-control and Ag film formation is rather trivial; as long as laser light is irradiated the density of Ag grains on the surface gradually increases.

We will show that if we change some parameters of model, for instance, a parameter b which denotes the incident light power per site, then there occurs a transition from State B to State A, and then the self-controlled formation of Ag file is realized. We remark that in the real experiments the p-n junction was reversely biased with a fixed voltage ($V_b = -1.5$ V). Therefore, the positive charge on the Ag surface is bounded and it will be saturated. In order to simplify the model, however, we do not take into account such an effect in the present study.

The paper is organized as follows. In Sec.2 the setting of the present model, the algorithm of processes, and the quantities which we will calculate are explained. The results of numerical simulations are given in Sec.3. There properties of the dynamical transition of surface state are studied by the analogy of equilibrium phase transitions associated with critical phenomena [11, 12, 13]. Sec. 4 is devoted to concluding remarks.

2 Discrete-Time Stochastic Model on a Lattice

Let L be an integer and consider an $L \times L$ square lattice $\Lambda_L = \{1, 2, \dots, L\}^2$. For two sites $\mathbf{r} = (x, y)$, $\mathbf{r}' = (x', y') \in \Lambda_L$ with distance $|\mathbf{r} - \mathbf{r}'| \equiv \sqrt{(x - x')^2 + (y - y')^2} = 1$, we say that they are the nearest-neighbor sites. We consider a stochastic process with a discrete time $t \in \mathbb{N}_0 \equiv \{0, 1, 2, \dots\}$. Here a particle will represent a positively charged Ag grain. At each time $t \in \mathbb{N}_0$, the following two kinds of stochastic variables will be defined,

$$\begin{aligned} n_t(\mathbf{r}) &= \text{the number of deposited particles at site } \mathbf{r}, \\ q_t(\mathbf{r}) &= \text{the amount of charge at site } \mathbf{r}, \end{aligned} \tag{2.1}$$

$\mathbf{r} \in \Lambda_L$, where $n_t(\mathbf{r}) \in \mathbb{N}_0$ and $q_t(\mathbf{r}) \in \mathbb{R}_+ \equiv \{x \in \mathbb{R} : x \geq 0\}$ (the set of nonnegative real numbers). At each time $t \in \mathbb{N}_0$, a collection of pairs of these stochastic variables over the lattice gives a *configuration* of the process, which is denoted by

$$\xi_t = \{(n_t(\mathbf{r}), q_t(\mathbf{r})) : \mathbf{r} \in \Lambda_L\}, \quad t \in \mathbb{N}_0. \tag{2.2}$$

In a given configuration ξ_t, if $n_t(\mathbf{r}) \geq 1$ and $n_t(\mathbf{r}') \geq 1$ for a pair of the nearest-neighbor sites $(\mathbf{r}, \mathbf{r}')$, we say that these two sites are *connected*. Moreover, for a pair of sites $\mathbf{r}$ and $\mathbf{r}'$ with $|\mathbf{r} - \mathbf{r}'| > 1$, if there is a sequence of sites $\mathbf{r}_0 \equiv \mathbf{r}, \mathbf{r}_1, \dots, \mathbf{r}_{n-1}, \mathbf{r}_n \equiv \mathbf{r}'$ in Λ_L with $|\mathbf{r}_j - \mathbf{r}_{j-1}| = 1, 1 \leq j \leq n$, $n \in \{2, 3, \dots\}$ such that any pair of successive sites $(\mathbf{r}_{j-1}, \mathbf{r}_j), 1 \leq j \leq n$ are connected, then we also say that $\mathbf{r}$ and $\mathbf{r}'$ are *connected*. For each site $\mathbf{r}$ with $n_t(\mathbf{r}) \geq 1$, a two-dimensional *cluster* including the site $\mathbf{r}$ is defined by

$$C_t(\mathbf{r}) = \{\mathbf{r}' \in \Lambda_L : \mathbf{r} \text{ and } \mathbf{r}' \text{ are connected}\}. \tag{2.3}$$

By definition, if $\mathbf{r}$ and $\mathbf{r}'$ are connected, then $C_t(\mathbf{r}) = C_t(\mathbf{r}')$. The total number of sites $\mathbf{r}'$ included in $C_t(\mathbf{r})$ is denoted by $|C_t(\mathbf{r})|$, which represents an area on Λ_L of the cluster of deposited particles.

We introduce the parameters in $\mathbb{R}_+$ as

$$\begin{aligned} b &= \text{incident light power per site,} \\ a &= \text{effective coupling constant of} \\ &\quad \text{a repulsive Coulomb potential between charges,} \\ E_{\rm th} &= \text{threshold energy for deposition on the surface.} \end{aligned} \tag{2.4}$$

If the kinetic energy of Ag^+ grain injected to the surface by RF sputtering is relatively small, the deposition on the surface will be inhibited by the Coulomb repulsive force between the Ag^+ grain and the positively charged surface. In the present stochastic model, we do not calculate such electrodynamical processes and simply introduce two variables a and $E_{\rm th}$ as parameters. We set a function $f : \mathbb{N}_0 \mapsto \mathbb{R}$, which specifies the increment ratio of charge per site and per time-step as a function of cluster size to which the site belongs. We assume that f is given by (1.1) with positive constants s_0 and σ. Now we explain the elementary process, $\xi_t \mapsto \xi_{t+1}, t \in \mathbb{N}_0$.

Assume that a configuration ξ_t is given at time $t \in \{0, 1, 2, \dots\}$.

(i) Choose a site randomly in Λ_L. The chosen site is denoted by $\mathbf{x}$.

(ii) Calculate the repulsive Coulomb potential at $\mathbf{x}$ caused by all charges on Λ_L by

$$V(\mathbf{x}) = \sum_{\mathbf{r}\in\Lambda_L} a\frac{q_t(\mathbf{r})}{|\mathbf{x}-\mathbf{r}|_+}, \tag{2.5}$$

where $|\mathbf{x}|_+ = |\mathbf{x}|$, if $|\mathbf{x}| > 0$ and $|\mathbf{x}|_+ = 1$, if $|\mathbf{x}| = 0$. (Here we consider a 'coarse grain model', and thus any singularity of the Coulomb-potential function should be eliminated.)

(ii-1) If $V(\mathbf{x}) \le E_{\rm th}$, then a charged particle is deposited at the site $\mathbf{x}$;

$$n_{t+1}(\mathbf{r}) = \begin{cases} n_t(\mathbf{r}) + 1, & \mathbf{r} = \mathbf{x}, \\ n_t(\mathbf{r}), & \mathbf{r} \neq \mathbf{x}. \end{cases} \tag{2.6}$$

(ii-2) If $V(\mathbf{x}) > E_{\rm th}$, then let $\mathbf{y}_0 = \mathbf{x}$ and calculate $V(\mathbf{y})$ at every nearest-neighbor site of $\mathbf{y}_0$, $\mathbf{y} \in \mathcal{N}(\mathbf{y}_0) \equiv \{\mathbf{y} \in \Lambda_L : |\mathbf{y} - \mathbf{y}_0| = 1\}$. If the site which attains $\min_{\mathbf{y}\in\mathcal{N}(\mathbf{y}_0)} V(\mathbf{y})$ is uniquely determined, let that site be $\mathbf{y}_1$. When the minimum is attained by plural sites, we choose one of them randomly and let it be $\mathbf{y}_1$. If $V(\mathbf{y}_1) > V(\mathbf{y}_0)$, then we regard that the particle is repulsed from the charged surface and cannot be deposited. Hence the configuration is not changed at all,

$$n_{t+1}(\mathbf{r}) = n_t(\mathbf{r}), \quad {}^\forall\mathbf{r} \in \Lambda_L. \tag{2.7}$$

If $V(\mathbf{y}_1) \le E_{\rm th}$, we set $\mathbf{x}^* = \mathbf{y}_1$. If $E_{\rm th} < V(\mathbf{y}_1) \le V(\mathbf{y}_0)$, calculate $V(\mathbf{y})$ at every $\mathbf{y} \in \mathcal{N}(\mathbf{y}_1)$ and follow the same procedure as above to determine a site $\mathbf{y}_2$. If $V(\mathbf{y}_2) > V(\mathbf{y}_1)$, the deposition is not done and we have (2.7). If $V(\mathbf{y}_2) \le E_{\rm th}$, set $\mathbf{x}^* = \mathbf{y}_2$. If $E_{\rm th} < V(\mathbf{y}_2) \le V(\mathbf{y}_1)$, we repeat the similar procedure to those explained above. When $\mathbf{x}^* \in \Lambda_L$ is determined, the charged particle is deposited at the site $\mathbf{x}^*$;

$$n_{t+1}(\mathbf{r}) = \begin{cases} n_t(\mathbf{r}) + 1, & \mathbf{r} = \mathbf{x}^*, \\ n_t(\mathbf{r}), & \mathbf{r} \neq \mathbf{x}^*. \end{cases} \tag{2.8}$$

Each sequence $\mathbf{x} = \mathbf{y}_0 \to \mathbf{y}_1 \to \cdots \to \mathbf{y}_n = \mathbf{x}^*$ with some $n \in \{1, 2, \dots\}$ simulates a path of *drift process* on the surface performed by a particle before it is deposited at $\mathbf{x}^*$

(iii) Clusters at time $t+1$, $\{C_{t+1}(\mathbf{r}) : \mathbf{r} \in \Lambda_L\}$ are redefined for the configuration $\{n_{t+1}(\mathbf{r}) : \mathbf{r} \in \Lambda_L\}$ given by (ii). For each cluster $C_{t+1}(\mathbf{r})$, the accumulated total charge has been $\sum_{\mathbf{r}' \in C_{t+1}(\mathbf{r})} q_t(\mathbf{r}')$. In addition to that, the following amount of charge is added; $b|C_{t+1}(\mathbf{r})| f(|C_{t+1}(\mathbf{r})|)$. (See Eq.(1.1) and the explanation given above it.) Then the charge at site $\mathbf{r}$ at time $t+1$ is given by

$$q_{t+1}(\mathbf{r}) = \frac{1}{|C_{t+1}(\mathbf{r})|} \left\{ \sum_{\mathbf{r}' \in C_{t+1}(\mathbf{r})} q_t(\mathbf{r}') + b|C_{t+1}(\mathbf{r})| f(|C_{t+1}(\mathbf{r})|) \right\}, \quad \mathbf{r} \in \Lambda_L. \tag{2.9}$$

We note that the charge distribution in cluster can be spatially inhomogeneous in general depending on the shape of cluster on the surface. We have assumed the uniform distribution in (2.9), however, since keeping the model simple we would like to report the advantage of introducing the variable $q_t(\mathbf{r})$, which was not considered in the previous cellular automaton model [14], in order to realize transitions between the two distinct particle-deposition states.

We start at the empty configuration $\xi_0 = \{(n_0(\mathbf{r}), q_0(\mathbf{r})) = (0,0) : \mathbf{r} \in \Lambda_L\}$ and observe the following quantities at times $t \in \{0, 1, 2, \dots, T\}$ with a sufficiently large T,

$$\begin{aligned} A_t &= \sum_{\mathbf{r} \in \Lambda_L} \mathbf{1}(n_t(\mathbf{r}) \ge 1), \\ Q_t &= \sum_{\mathbf{r} \in \Lambda_L} q_t(\mathbf{r}), \end{aligned} \tag{2.10}$$

where $\mathbf{1}(\omega)$ is an indicator function of a condition ω; $\mathbf{1}(\omega) = 1$ if ω is satisfied, and $\mathbf{1}(\omega) = 0$ otherwise. The quantity A_t shows the *total area of clusters* at time t and Q_t the *total charge* of particles deposited on the surface Λ_L at time t. We set

$$R_t = \frac{A_t}{L^2}, \tag{2.11}$$

which denotes the *occupation ratio* by deposition on the surface at time t. We also define

$$Q_t^{(T)} = \frac{Q_t}{Q_T}, \quad t \in \{0, 1, 2, \dots, T\} \tag{2.12}$$

with a given T.

3 Simulation Results

We performed computer simulation of the stochastic model. Here we fix the following parameters as

$$a = 1 \times 10^{-3}, \quad s_0 = 12, \quad \sigma = 2, \tag{3.1}$$

and

$$L = 64, \quad T = 10^4. \tag{3.2}$$

The parameters b and $E_{\rm th}$ are changed and dependence of the process on them is studied. (We will also discuss the results on systems with different sizes L in Sec.3.3 and Sec.4.)

3.1 Two states

Figure 3 shows time dependence of the occupation ratios by deposition on the surface, R_t (solid lines), and the total charges on the surface normalized by the values at $t = T$, $Q_t^{(T)}$ (broken lines), for $b = 0.01, 0.10, 0.30, 0.50, 0.70$, and 0.90, when we set $E_{\rm th} = 10$. When b is small ($b = 0.01, 0.10$ and 0.30), R_t increases monotonically and $Q_t^{(T)}$ shows saturation after some time-period. When b is large ($b = 0.50 - 0.90$), on the other hand, R_t shows saturation in time, while $Q_t^{(T)}$ increases monotonically. The results implies when b is small the system is in State B, while b is large in State A. The critical value of b will be evaluated in the next subsection as $b_{\rm c} = 0.44$ in this case with $E_{\rm th} = 10$.

3.2 Order parameter and critical exponent

When the system is in State B, R_t increases monotonically and $\lim_{t\to\infty} R_t \simeq 1$, that is, the surface will be almost covered by particles. On the other hand, in State A, the deposition is suppressed by Q_t which increases monotonically in time and the surface formation is self-controlled. As a result we will have a nontrivial steady state, in which $\lim_{t\to\infty} R_t = R_\infty < 1$.

The vacant-site density on the surface in the steady state is defined as

$$\rho_0 \equiv 1 - R_\infty. \tag{3.3}$$

It will play a role as an *order parameter* for the transition from State B to State A.

Here ρ_0 is approximated by the value $\rho_0^{(T)} \equiv 1 - R_T$ at $T = 10^4$. For each choice of parameters, we performed ten independent simulations and studied the averaged values of $\rho_0^{(T)}$. Figure 4 shows dependence of $\rho_0^{(T)}$ on b for $E_{\rm th} = 5, 10, 20, 30, 40$, and 50. There $\rho_0^{(T)}$'s seem to behave as continuous functions of b. It implies that the transition is continuous and the critical value $b_{\rm c} = b_{\rm c}(E_{\rm th})$ will be defined by

$$\begin{aligned} b_{\rm c}(E_{\rm th}) &= \max\{b > 0 : \rho_0(E_{\rm th}, b) = 0\}, \\ &= \min\{b > 0 : \rho_0(E_{\rm th}, b) > 0\}. \end{aligned} \tag{3.4}$$

Figure 5 shows the b-dependence of $Q_T = Q_T(E_{\rm th}, b)$ for $E_{\rm th} = 5, 10, 20, 30, 40$, and 50. The result implies that, for $b < b_{\rm c}(E_{\rm th})$, $\lim_{t\to\infty} Q_t < \infty$, while for $b > b_{\rm c}(E_{\rm th})$,

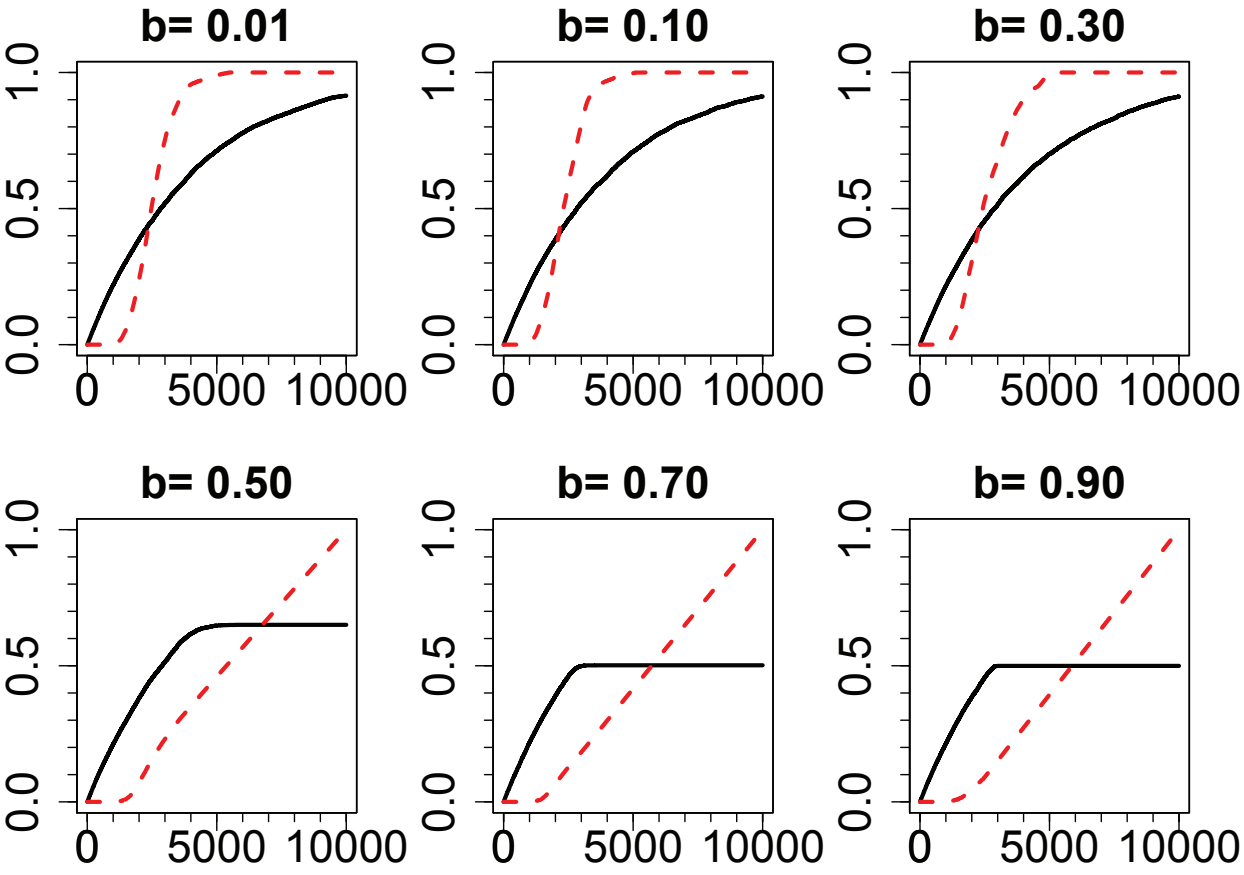

Figure 3: R_t (solid lines) and $Q_t^{(T)}$ (broken lines) are shown as functions of time-steps $t \in \{0, 1, \ldots, T\}$ with $T = 10^4$ for $b = 0.01, 0.10, 0.30, 0.50, 0.70$, and 0.90, where we set $E_{\text{th}} = 10$. The abscissas show time steps.

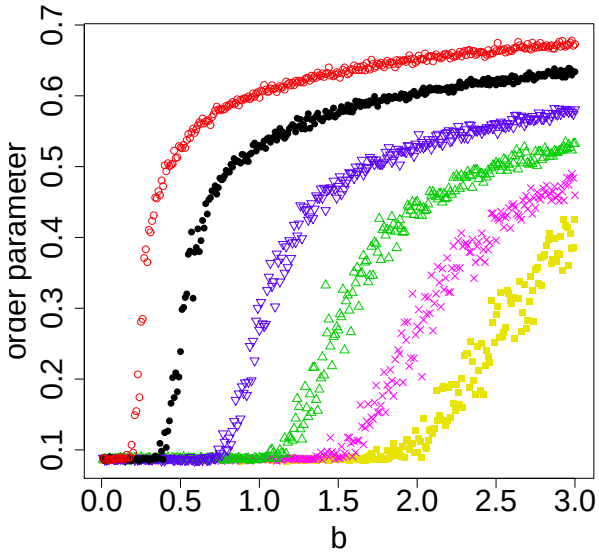

Figure 4: Order parameters as functions of b for $E_{\rm th} = 5$ (denoted by $\circ$), 10 ($\bullet$), 20($\bigtriangledown$), 30($\bigtriangleup$), 40($\times$), and 50($\square$).

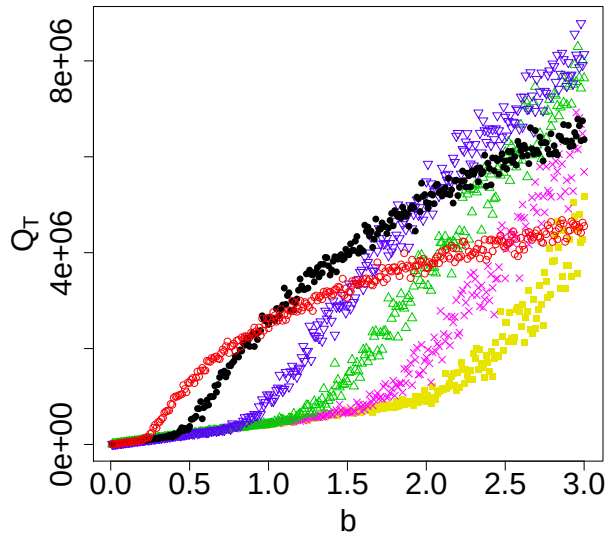

Figure 5: Q_T with $T = 10^4$ versus b for $E_{\rm th} = 5$ (denoted by $\circ$), 10 ($\bullet$), 20($\bigtriangledown$), 30($\bigtriangleup$), 40($\times$), and 50($\square$).

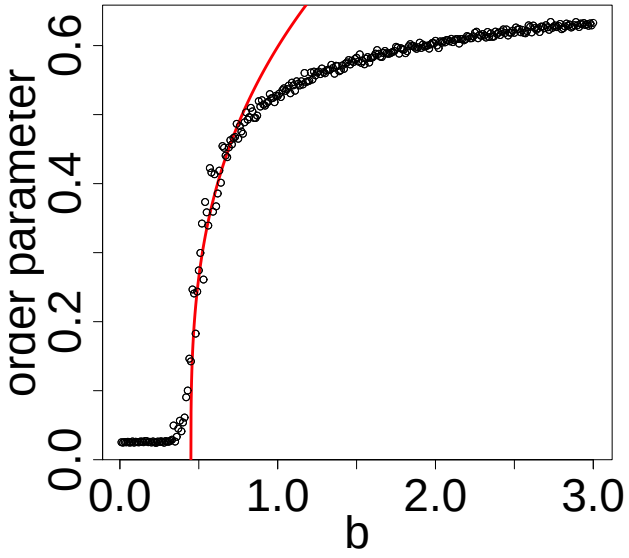

Figure 6: Simulation result of the order parameter ρ_0 for $E_{\rm th} = 10$. The curve shows (3.6) with $b_{\rm c} = 0.44$ and $\beta = 0.34$. In the vicinity of critical value $b_{\rm c}$ in State A, the power-law behavior (3.6) is observed.

$\lim_{t\to\infty} Q_t = \infty$ (see the remark given at the end of Sec.1). Thus the critical value $b_{\rm c}(E_{\rm th})$ is also characterized as

$$\begin{aligned} b_{\rm c}(E_{\rm th}) &= \max\left\{b > 0 : \lim_{t\to\infty} Q_t < \infty\right\}, \\ &= \min\left\{b > 0 : \lim_{t\to\infty} Q_t = \infty\right\}. \end{aligned} \tag{3.5}$$

As an analogy of the second-order phase transitions associated with critical phenomena in the equilibrium statistical mechanics, singular behavior of the order parameter in the vicinity of transition point $b_{\rm c}$ in State A is expected to be described by the following power-law,

$$\rho_0 \sim (b - b_{\rm c})^{\beta}, \quad 0 < b - b_{\rm c} \ll 1, \tag{3.6}$$

with an exponent β [11, 12, 13].

For each value of $E_{\rm th}$, we performed the numerical fitting of the data to the power-law (3.6) and evaluated values of $b_{\rm c}$ and β. For example, the curve in Fig. 6 shows the obtained curve (3.6) by fitting the data for $E_{\rm th} = 10$, which gives $b_{\rm c} = 0.44$ and $\beta = 0.34$. As we will report in the next subsection, the critical value $b_{\rm c}$ depends on $E_{\rm th}$, but we found that the dependence of evaluated β on $E_{\rm th}$ is very small; $\beta = 0.31$-0.39 for $E_{\rm th} = 5$-50.

3.3 Critical line between State A and State B

We have evaluated the critical values $b_{\rm c} = b_{\rm c}(E_{\rm th})$ as $b_{\rm c}(5) = 0.22, b_{\rm c}(10) = 0.44, b_{\rm c}(20) = 0.90, b_{\rm c}(30) = 1.30, b_{\rm c}(40) = 1.75$, and $b_{\rm c}(50) = 2.25$, respectively. They are plotted by cross

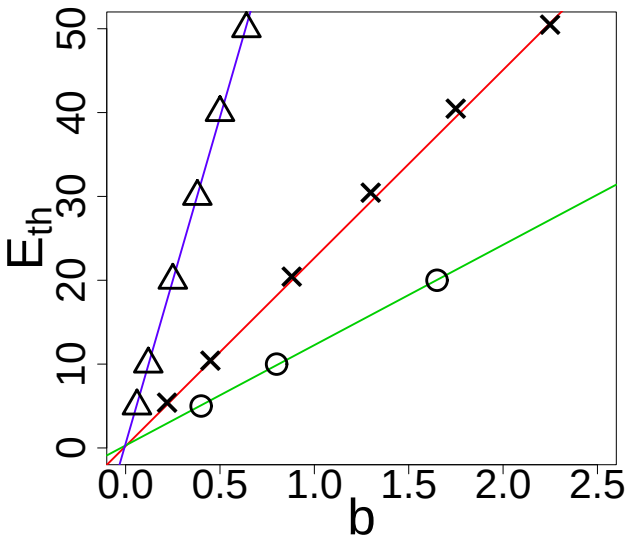

Figure 7: The values of b_c of several E_{th}'s are shown by $\times$'s for the system with size $L = 64$. The critical line is well described by a straight line, $b_c = c(L)E_{th}$ with $c(L = 64) \simeq 0.045$, which divides State A (the lower right region) from State B (the upper left region). The critical values evaluated for the systems with sizes $L = 50$ and $L = 100$ are also plotted by $\bigcirc$'s and $\triangle$'s, respectively. We have evaluated the coefficients of critical lines as $c(50) \simeq 0.084$ and $c(100) \simeq 0.013$.

marks in Fig. 7. We can see that the *critical line* is well described by a straight line,

$$b_c = cE_{th} \quad \text{with } c \simeq 0.045. \tag{3.7}$$

As discussed in Sec.4, the critical value $b_c(E_{th})$ also depends on the lattice size L. Because of the long-ranged Coulomb potential (2.5), $b_c(E_{th})$ decreases monotonically as L increases. In other words, the coefficient in (3.7) is L-dependent; $c = c(L)$, and $\lim_{L\to\infty} c(L) = 0$. In this sense, the transitions between State A and State B are not usual phase transitions, which should be defined in infinite-size (thermodynamic) limits. Therefore, Fig. 7 cannot be regarded as a phase diagram. In the present study, we are interested in transitions in nonequilibrium states found on a surface of device with a mesoscopic scale. The values themselves of $b_c(E_{th})$ as well as $c(L)$ reported here are not so important, since they change depending on system size. Our preliminary study by numerical simulations for different lattice sizes imply, however, that the linear dependence of b_c on E_{th} is universal as far as the system size is large but finite as shown in Fig. 7. Note that validity of the power-law (3.6) has been numerically confirmed also for different sizes of L with $\beta \simeq 0.3$.

Figure 8: Cluster structure formed in the steady state, when $(E_{\rm th}, b) = (10, 0.65)$. Occupied sites are dotted.

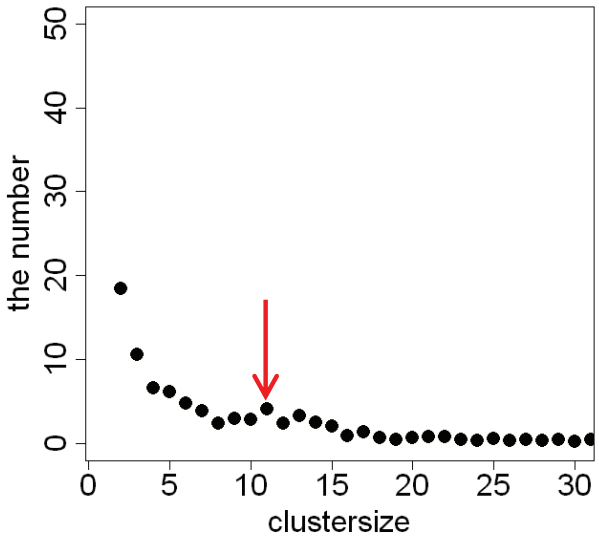

Figure 9: Cluster-size distribution in the steady state, when $(E_{\rm th}, b) = (10, 0.65)$. As indicated by an arrow, a peak is found around $s \simeq 11$.

3.4 Cluster structures in State A

For $(E_{\rm th}, b) = (10, 0.65)$, a configuration of clusters on the surface obtained in the steady state (at $T = 10^4$) is plotted in Figure 8, where occupied sites by particles are dotted. For $E_{\rm th} = 10$, we have estimated $b_{\rm c} = 0.44$. Then this figure shows a self-controlled surface-configuration realized in State A. Averaging over ten independent simulations, distribution of cluster size $|C_T(\mathbf{r})|$ on the steady-state surface in State A is calculated. Figure 9 shows it for $(E_{\rm th}, b) = (10, 0.65)$. A peak is found around $s \simeq 11$, which is consistent with our choice of parameter $s_0 = 12$ in the simulation. The present results are consistent with the experimental observation reported by [5] as well as the simulation results by [14].

4 Concluding Remarks

In the present paper we generalized the cellular automaton model [13] by Naruse et al. [14] and proposed a new stochastic model to describe the nonequilibrium dynamics of Ag-film pattern formation on an electrode of the photovoltaic device of Yukutake et al. [5]. In the present new model, not only the number of deposited particle $n_t(\mathbf{r})$ but also the amount of charge $q_t(\mathbf{r})$ are considered as stochastic variables at each site $\mathbf{r}$ in the $L \times L$ square lattice at time $t \in \mathbb{N}_0$. The previous model used the 'pseudo footprint' method to take into account the repulsive interaction between an Ag^+ ion approaching the surface and positively charged Ag clusters on the surface. In the present algorithm of model, the repulsive Coulomb potential at each site caused by all charges on the lattice except the site is exactly calculated at each time-step, and drift and deposition processes are simulated. The essential improvement of the model is such that we include the effect of optical near-fields generated by light-matter interaction by introducing a parameter b and a function $f(s)$. There b denotes the incident light power per site on the lattice and $f(s)$ expresses the size-dependent resonance effect of optical near-fields on matter-size s. We have regarded b as an external control parameter of the model. We have shown that, as b increases, there occurs a transition of the surface state of pattern formation with a critical value $b_{\rm c}$, such that if $b \leq b_{\rm c}$ the optical near-fields are not induced effectively (State B), while if $b > b_{\rm c}$ they are induced effectively and Ag deposition process is self-controlled (State A). A nontrivial and unique Ag film is formed in State A, while in State B random Ag-deposition will be continued as long as the simulation is continued. We have discussed the transitions of surface processes from State B to State A by the analogy of equilibrium second-order phase transitions with critical phenomena [11, 12, 13]. We also studied the dependence of $b_{\rm c}$ on the threshold energy $E_{\rm th}$ for elementary deposition of single Ag^+ on the surface.

The transition of surface state discussed in this paper is not a phase transition in the usual sense, since our model is defined on a lattice with a finite size $L < \infty$; $L = 64$ for the simulation data reported above. In equilibrium and hence in stable systems the $L \to \infty$ limit will provide the thermodynamic limit and it describes macroscopic behavior of materials. In the present model, however, the direct $L \to \infty$ limit may be meaningless, since the repulsive Coulomb repulsive potential (2.5) will diverge as $L \to \infty$ in the late stage of process in which sufficient amount of charge is accumulated on the surface. (It implies that $b_{\rm c}$ should be a

decreasing function of L, since $V(\mathbf{x})$ given by (2.5) will take larger value as L increases, and $b_c \to 0$ as $L \to \infty$ for all $E_{th} > 0$.) In the present study, we are interested in nonequilibrium deposition dynamics of charged particles on mesoscopic materials. We should assume that the system size L of model is sufficiently large but finite.

From the view point of study of nonequilibrium statistical mechanics [11, 12, 13], it is an interesting problem to find a relevant scaling limit which can realize the present transitions of surface state as nonequilibrium phase transitions. A preliminary study by changing the lattice size L in numerical simulations implies that the parameter b should be scaled as $b = b_0 L^{-(2+\nu)}$ with a constant b_0 and a scaling exponent ν in the infinite-size limit $L \to \infty$. The dependence of $c(L)$ on L reported in Fig. 7 is consistent with it and gives a preliminary estimate $\nu \simeq 0.7$. Such a mathematical physics aspect of the present model is also interesting and will be reported elsewhere.

Acknowledgements The present authors would like to thank S. Tojo for useful discussions on the present work. This study is supported by the Grant-in-Aid for Challenging Exploratory Research (No.15K13374) of Japan Society for the Promotion of Science. MK is supported in part by the Grant-in-Aid for Scientific Research (C) (No.26400405) of Japan Society for the Promotion of Science.

References

[1] M. Ohtsu, T. Kawazoe, T. Yatsui, and M. Naruse, IEEE J. Sel. Top. Quantum Electron. **14**, 1404 (2008).

[2] S. Tojo and M. Hasuo, Phys. Rev. A **71**, 012508 (2005).

[3] M. Ohtsu, *Dressed Photons: Concepts of Light-Matter Fusion Technology*, Nano-Optics and Nanophotonics (Springer, Berlin, 2014).

[4] T. Franzl, T. A. Klar, S. Schietinger, A. L. Rogach, and J. Feldmann, Nano Lett. **4**, 1599 (2004).

[5] S. Yukutake, T. Kawazoe, T. Yatsui, W. Nomura, K. Kitamura, and M. Ohtsu, Appl. Phys. B **99**, 415 (2010).

[6] C. Pistol, C. Dwyer, and A. R. Lebeck, IEEE MICRO **28**, 7 (2008).

[7] T. Kawazoe, M. A. Mueed, and M. Ohtsu, Appl. Phys. B **104**, 747 (2011).

[8] M. Naruse, N. Tate, M. Aono, and M. Ohtsu, Rep. Prog. Phys. **76**, 056401 (2013).

[9] M. Naruse, ed., *Nanophotonics Information Physics: Nanointelligence and Nanophotonics Computing*, Nano-Optics and Nanophotonics (Springer, Berlin, 2014).

[10] T. Yatsui, W. Nomura, and M. Ohtsu, Nano Letters **5**, 2548 (2005).

[11] J. Marro and R. Dickman, *Nonequilibrium Phase Transitions in Lattice Models*, (Cambridge University Press, Cambridge, 1999).

[12] R. Mahnke, J. Kaupužs, and I. Lubashevsky, *Physics of Stochastic Processes: How Randomness Acts in Time*, (Wiley-VCH, Germany, 2009).

[13] B. Chopard and M. Droz, *Cellular Automata Modeling of Physical Systems*, (Cambridge University Press, Cambridge, 1998).

[14] M. Naruse, T. Kawazoe, T.Yatsui, N. Tate, and M. Ohtsu, Appl. Phys. B **105**, 185 (2011).

[15] K. Kobayashi, S. Sangu, H. Ito, and M. Ohtsu, Phys. Rev. A **63**, 013806 (2000).